IEEE Access
Multidisciplinary | Rapid Review | Open Access Journal

Received May 17, 2022, accepted June 1, 2022, date of publication June 8, 2022, date of current version June 17, 2022.

Digital Object Identifier 10.1109/ACCESS.2022.3181178

Robust Energy-Efficient Hybrid Beamforming Design for Massive MIMO LEO Satellite Communication Systems

YANG LIU, CHANGQING LI, JIONG LI, AND LU FENG
School of Space Information, Space Engineering University, Beijing 101416, China

Corresponding author: Jiong Li (lij_2015@126.com)

This work was supported by the National Natural Science Foundation of China under Grant 62001516.

ABSTRACT In low earth orbit (LEO) satellite communication systems, the limited energy supply capacity and the difficulty in obtaining channel state information (CSI) are the practical challenges. Motivated by this, we focus on the design of robust hybrid beamforming to maximize the energy efficiency of LEO satellite communication systems. Assuming that the LEO satellite transmitter adopts the massive multi-input multi-output (MIMO) technology, considering the CSI errors caused by propagation delay and Doppler shift, under the constraints of transmit power and quality of service (QoS), a robust energy-efficient hybrid beamforming scheme is proposed. Since that there are no explicit expressions for the ergodic user rate and the ergodic signal-to-interference-plus-noise ratio, the approximate values with closed-form expressions are adopted. Then, we invoke the semidefinite programming (SDP) algorithm to transform the nonconvex quadratic constrained quadratic programming (QCQP) problem equivalently, and an inner and outer nested iterative algorithm combining quadratic transformation fractional programming (QTFP) and concave convex process (CCCP) is utilized to transfer a nonconvex problem into a convex problem. Meanwhile, we adopt a penalty function algorithm to solve the rank-one constraint in semidefinite programming algorithm. Finally, we invoke the normal form distance minimization (NFDM) algorithm and the alternating optimization (AltOpt) algorithm to jointly solve the digital beamforming matrix and analog beamforming matrix in hybrid beamformer. Numerical results validate that our proposed robust approach significantly outperforms the conventional one.

INDEX TERMS Low earth orbit satellite communication systems, massive MIMO, energy efficiency, robust, hybrid beamforming.

I. INTRODUCTION

Low earth orbit (LEO) satellite communication systems have the advantages of wide coverage, full connectivity, low latency, and large capacity in the field of satellite communications [1], which have recently become a research hotspot [2]. LEO satellite communication systems would become effective supplements to terrestrial mobile communication systems, which can solve the communication problems in remote areas, oceans, space, deserts and other areas that cannot be covered by terrestrial mobile communication systems. In addition, when terrestrial communication facilities are damaged by natural disasters, such as earthquakes and floods, LEO satellite communication systems can serve as an emergency communication means. At present, the construction and development of LEO satellite communication systems have received attention and investment from major countries.

With the growth of the number of mobile terminals and the improvement of the demand for communication performance, high communication rate and low power consumption have become important reference indicators for the future communication system design. In particular, for LEO satellite communication systems, the energy supply capacity is limited. To extend the service life of satellites and strengthen the stability of the system, it is necessary to pay attention to the optimization of energy efficiency (EE), EE has become an important perspective for the researches of LEO satellite communication systems [3]. In [4], considering channel state information (CSI) errors, the authors investigated a robust

The associate editor coordinating the review of this manuscript and approving it for publication was Wei Feng.

digital beamforming algorithm of multi-beam LEO satellite IoT, with the optimization objective of minimizing the total power consumption. In [5], based on the statistical CSI, a beamforming algorithm for maximizing resource efficiency of the massive multiple-input multiple-output (MIMO) system was investigated, and the trade-off between system spectral efficiency (SE) and EE was considered in the scheme. In [6], considering CSI errors, a robust beamforming design for maximizing resource efficiency of multi-beam satellites was investigated. In [7], based on the statistical CSI, a hybrid beamforming design for EE maximization of LEO satellite communication systems was studied, but the authors did not take the CSI errors into consideration. In [8], based on the perfect CSI, a digital precoding design of multi-beam satellites was studied, with the optimization objective of maximizing EE, considering the constraints of the transmit power and quality of service (QoS). In [9], considering the CSI errors, with the optimization objective of minimizing the total power consumption, a robust sequential optimization algorithm was proposed, which implemented the digital precoding design of multi-beam satellites while ensuring the EE constraints of each group of users. In [10], considering the CSI errors, the authors investigated a robust zero-forced precoding design for multi-beam satellites to improve system EE.

In this paper, we propose a transmission scheme with full frequency reuse (FFR) for LEO satellite communication systems [11], which will introduce severe inter-beam interference. Massive MIMO beamforming technology is a core technology of 5G [12], which can provide the rich spatial freedom, support the space division multiple access (SDMA) and multiplexing of time-frequency resources, and greatly reduce the inter-beam interference. Therefore, we focus on the hybrid beamforming design for LEO satellite communication systems equipped with the Massive MIMO transmission technology.

It is worth noting that the following issues need to be considered in the beamforming design for LEO satellite communication systems:

- Due to the Doppler shift caused by the high mobility of LEO satellites, the channel estimation pilot pollution caused by the high channel dimensions of Massive MIMO transmission technology, and the channel phase perturbations caused by the long propagation delay between satellites and terminals, it is complex and difficult to obtain the instantaneous and accurate CSI [13]. Therefore, the robust beamforming design based on the imperfect CSI has important practical significance.
- The hardware cost and system complexity of the digital beamforming architecture are high, and the volume and weight are large, so it is not suitable for LEO satellite communication systerms. Although the hardware cost of the hybrid beamforming architecture based on the partial connection structure is low, the system capacity is lower than that of the full connection structure, which can not meet the future high-speed rate communication requirement. Therefore, we comprehensively consider the factors of energy efficiency and system capacity, the hybrid beamforming architecture based on the full connection structure is a cost-effective choice [14].
- Due to the limited energy supply capacity on the LEO satellites, the transmit power constraint of the transmitter should be considered. And the QoS of various terminals are different, the signal-to-interference-plus-noise ratio (SINR) constraint of each user should be taken into account.

In conclusion, aiming at maximizing the EE, we focus on the robust energy-efficient hybrid beamforming design for LEO satellite communication systems. The major contributions of the current work are summarized as follows:

- We introduce Massive MIMO transmission technology into LEO satellite communication systems. And assuming that the satellite transmitter is equipped with a uniform plane array (UPA), we establish the downlink model of LEO satellite communication systems.
- We establish the Massive MIMO channel model for LEO satellite communication systems by incorporating the LEO satellite signal propagation properties. Meanwhile, we analyze the effects of propagation delay and Doppler shift on the CSI.
- Due to the CSI errors, the ergodic user rate and ergodic SINR can not be expressed explicitly. To this end, we adopt the explicit tight approximations of the two ergodic expressions.
- For the quadratic constrained quadratic programming (QCQP) optimization problem, to simplify the problem modeling, we adopt the semidefinite programming (SDP) algorithm to transform the optimization problem equivalently.
- To solve the problem of sum-of-ratios fractional programming form and the nonconvex characteristic in the objective function, we propose an inner and outer nested iteration algorithm combining quadratic transformation fractional programming (QTFP) and concave convex process (CCCP) to transfer the objective function into a concave function. Then, we adopt the convex optimization algorithm to solve the problem.
- To handle the rank-one constraint problem existing in the SDP algorithm, we adopt a penalty function algorithm.
- To obtain the digital beamforming matrix and the analog beamforming matrix in the hybrid beamformer, we adopt the low-complexity alternating optimization (AltOpt) algorithm on the basis of the normal form distance minimization (NFDM) algorithm.
- Simulation results show that the robust algorithm proposed in this paper has a fast convergence speed and a significant performance gain compared with the conventional non-robust algorithm.
- For LEO satellite communication systems, we introduce the Massive MIMO transmission technology, which can improve the spatial resolution, spectral efficiency and energy efficiency. Meanwhile, aiming at the influence

of CSI errors, we propose a robust method, which can improve the reliability of the communication system. Therefor, the proposed method can be suitable for the high-frequency band, high bandwidth, high-speed rate and high mobility communication scenario.

Note that The major notations adopted in the paper is listed in Table 1 for ease of reference.

TABLE 1. Notations list.

Notation	Definition
M_X, M_Y	Numbers of antennas of UPA
K	Number of users
N_{RF}	Number of RF links
$\boldsymbol{W}_{BB}$	Digital beamforming matrix
$\boldsymbol{W}_{RF}$	Analog beamforming matrix
$\boldsymbol{h}_k$	Downlink channel vector
n_k	Additive white Gaussian noise
$\boldsymbol{B}$	Hybrid beamforming matrix
$\boldsymbol{b}_k$	Hybrid beamforming vector
L_k	Number of multipaths
$g_{k,l}$	Complex channel gain
$f_{k,l}$	Doppler shift
$\tau_{k,l}$	Propagation delay
$\boldsymbol{a}_{k,l}$	Array response vector
$\boldsymbol{p}_f$	Error matrix caused by residual Doppler shift
$\boldsymbol{p}_{f_k}$	Error vector caused by residual Doppler shift
$\boldsymbol{e}_\theta$	Phase error matrix caused by residual delay
$\boldsymbol{e}_{\theta_k}$	Phase error vector caused by residual delay
$\varphi_{k,l}, \gamma_{k,l}$	Space angles
LP_{fs}	Free space path loss
LP_{at}	Atmospheric absorption loss
k_k	Rician factor
λ_k	Channel power
$SINR_k$	Signal-to-interference-plus-noise ratio
P_{total}	Total power consumption
P_T	Transmit power
P_0	Power consumption of circuit hardware
r_k	SINR constraint threshold
$\boldsymbol{W}_k$	Hybrid beamforming autocorrelation matrix
$\boldsymbol{H}_k$	Channel correlation matrix
$\boldsymbol{q}_{\theta_k}$	Error vector caused by residual delay
$\boldsymbol{Q}_{\theta_k}$	Expectation of autocorrelation matrix of $\mathfrak{q}_{\theta_k}$
$\boldsymbol{P}_{f_k}$	Expectation of autocorrelation matrix of $\mathfrak{p}_{f_k}$
$V_k^{te}(\boldsymbol{W})$	First-order Taylor expansion $V_k(\boldsymbol{W})$
τ, μ, m	Iteration index
ξ	Penalty factor

II. SYSTEM MODEL

As depicted in Fig.1, we take the downlink of the LEO satellite communication system as the research scenario, and the LEO satellite is equipped with a UPA composed of $M = M_X \times M_Y$ antennas, where M_X and M_Y are the numbers of antennas on the x- and y-axes, respectively. The system serves K single-antenna users simultaneously. In this paper, the UPA

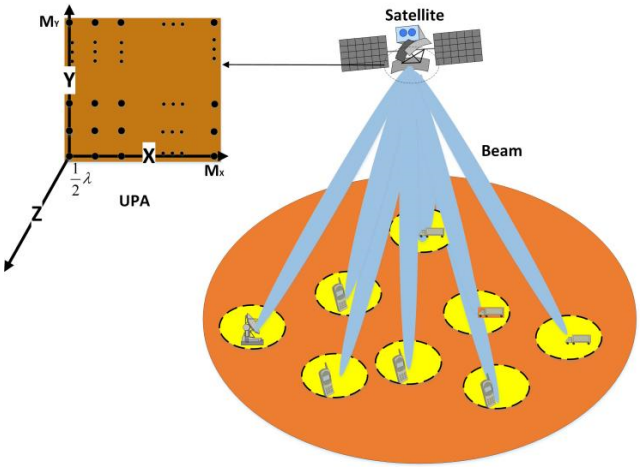

FIGURE 1. The downlink model of the LEO satellite communication system.

adopts the hybrid beamforming architecture based on the full connection structure. According to the characteristic of the fully connected hybrid beamforming architecture, the number of RF links of the UPA (N_{RF}) should be greater than or equal to the number of users, i.e., $N_{RF} \geq K$. And when $N_{RF} = 2K$, the spectral efficiency of the hybrid beamforming system is comparable to that of the digital beamforming system [14]. In this paper, we mainly investigate the hybrid beamforming design under the $N_{RF} = K$ condition.

The data streams at the LEO satellite transmitter are first processed by the digital beamformer for baseband processing, and then mapped to the UPA through the RF links for analog beamforming. Let $\boldsymbol{W}_{BB} \in \mathbb{C}^{K\times K} = [\boldsymbol{w}_{bb1}, \boldsymbol{w}_{bb2}, \ldots, \boldsymbol{w}_{bbK}]$ and $\boldsymbol{W}_{RF} \in \mathbb{C}^{M\times K} = [\boldsymbol{w}_{rf1}, \boldsymbol{w}_{rf2}, \ldots, \boldsymbol{w}_{rfK}]$ be the digital beamforming matrix and the analog beamforming matrix, respectively. Furthermore, the analog beamformer is implemented with phase shifters, which can only adjust the phases of the signals. So all non-zero elements of $\boldsymbol{W}_{RF}$ need to satisfy the unit modulus constraints, i.e., $\left|(\boldsymbol{W}_{RF})_{i,j}\right| = 1$. The received signal of the kth user is denoted as:

$$y_k = \boldsymbol{h}_k^H \boldsymbol{w}_{bbk} \boldsymbol{w}_{rfk} x_k + \sum\nolimits_{i\neq k} \boldsymbol{h}_k^H \boldsymbol{w}_{bbi} \boldsymbol{w}_{rfi} x_i + n_k, \quad \forall k \in [1, 2, \ldots, K] \tag{1}$$

where $\boldsymbol{h}_k \in \mathbb{C}^{M\times 1}$ represents the downlink channel vector from the UPA to the kth user, x_k represents the transmit signal for the kth user, which satisfies $\mathrm{E}\{x_k\} = 0, \mathrm{E}\left\{|x_k|^2\right\} = 1$, $\forall k \in K$. n_k denotes the additive white Gaussian noise of the kth user, which follows the distribution of $n_k \sim \mathbb{N}(0, N_0)$.

To facilitate analysis, let $\boldsymbol{B} \in \mathbb{C}^{M\times K} = \boldsymbol{W}_{RF}\boldsymbol{W}_{BB} = [\boldsymbol{b}_1, \boldsymbol{b}_2, \ldots, \boldsymbol{b}_K]$ be the hybrid beamforming matrix, let $\boldsymbol{b}_k = \boldsymbol{w}_{bbk}\boldsymbol{w}_{rfk}$ be the hybrid beamforming vector of the kth user.

III. CHANNEL MODEL

Considering the channel characteristics of Massive MIMO LEO satellite communication systems [15], [16], in this paper, we exploit statistical channel state information (sCSI).

The downlink channel vector from the LEO satellite transmitter to the kth user at instant t and frequency f can be represented by [17]

$$\boldsymbol{h}_k(t,f) = \sum_{l=1}^{L_k} g_{k,l} \cdot \exp\{j2\pi(tf_{k,l} - f\tau_{k,l})\} \cdot \boldsymbol{a}_{k,l}, \boldsymbol{h}_k(t,f) \in \mathbb{C}^{M\times 1} \tag{2}$$

where f represents the carrier frequency, L_k represents the number of channel propagation paths of the kth user, $g_{k,l}, f_{k,l}, \tau_{k,l}, \boldsymbol{a}_{k,l}$ represent the complex gain, Doppler shift, propagation delay, and UPA array response vector of path l, respectively. In the following, we mainly focus on three factors: Doppler shift, propagation delay, and array response.

A. DOPPLER SHIFT

The Doppler shift $f_{k,l}$ can not be ignored, which is mainly composed of the Doppler shift $f_{k,l}^{leo}$ caused by the satellite movement and the Doppler shift $f_{k,l}^{ut}$ caused by the terminal movement [18]. In practical communication systems, the Doppler shift is usually estimated by the frequency offset estimation method, and then Doppler shift precompensation is implemented [19]. The frequency offset estimation is generally divided into two stages: coarse estimation and fine estimation. During the coarse estimation stage, the user terminals calculate the Doppler shift at each moment based on the LEO satellite ephemeris and their own position information. As depicted in Fig. 2, the calculation formula is defined as:

$$f_{k,l}^{r} = f\frac{v}{c}\frac{\sin(\theta_l - \alpha)}{\sqrt{(\frac{R+H}{R})^2 + 1 - 2(\frac{R+H}{R})\cos(\theta_l - \alpha)}} \tag{3}$$

where c, f represent the speed of light and carrier frequency, respectively, v represents the vector of satellite motion velocity, θ_l represents the angle between the satellite motion direction and the signal propagation path l, R, H represent the earth's radius and orbital altitude, respectively, α represents the elevation angle of the user associated with path l. The coarse estimation can address the problem of large Doppler shift caused by the relative motion between the LEO satellite and user terminals. During the fine estimation stage, the users further calculate the Doppler shift $f_{k,l}^{p}$ by extracting and analyzing the pilot sequence. In conclusion, the value of Doppler shift estimation can be expressed as: $f_{k,l} = f_{k,l}^{r} + f_{k,l}^{p}$. Due to ephemeris errors, pilot estimation errors, and other factors, the Doppler shift estimation is usually inaccurate. After Doppler shift precompensation, there will still be residual Doppler shift, which can result in channel errors. The Cramer-Rao lower bound (CRLB) [20] of the Doppler shift for satellite communication systems can be expressed as:

$$\mathrm{CRLB}(f) = \frac{1}{\mathrm{SNR}}\frac{3}{2\pi^2 T^2 N(N^2-1)} \tag{4}$$

where SNR represents the signal-to-noise ratio, N, T represent the pilot symbol length and bit pulse length, respectively. According to the pilot overhead in the communication frame

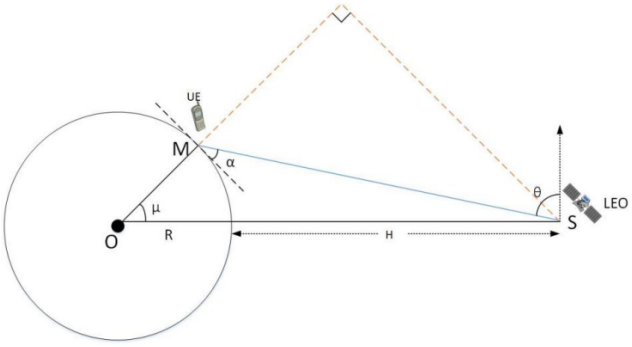

FIGURE 2. Schematic diagram of Doppler shift coarse estimate of the LEO satellite.

structure of LEO satellite communication systems, we can obtain the Cramer-Rao lower bound, which can be used as the variance σ_f^2 of residual Doppler shift after precompensation, and the maximum residual Doppler shift is randomly generated by using the variance and zero mean. Let the channel errors caused by residual Doppler shift be $\boldsymbol{p}_f = [\boldsymbol{p}_{f_1}, \boldsymbol{p}_{f_2}, \ldots, \boldsymbol{p}_{f_K}]^T, \boldsymbol{p}_{f_k} = [p_{f_{k,1}}, p_{f_{k,2}}, \ldots, p_{f_{k,M}}]^T$, which follow the distribution of *Jacks* [21].

B. PROPAGATION DELAY

Due to the large distance between the LEO satellite and user terminals (LEO satellite orbital altitude: 300km-2000km), the propagation delay is much larger than that of terrestrial mobile communication systems. To facilitate analysis, let $\tau_k^{\min} = \min\{\tau_{k,l}\}, \tau_k^{\max} = \max\{\tau_{k,l}\}$ represent the minimum propagation delay and the maximum propagation delay, respectively. Due to the long propagation delay of LEO satellite communication systems, it is almost impossible to obtain the instantaneous and accurate CSI. To receive the signal correctly, the delay precompensation with $\tau_{pc} = \beta\tau_k^{\min} + (1-\beta)\tau_k^{\max}, (0 \le \beta \le 1)$ value is usually carried out at the receivers. However, due to the randomness of propagation delay variation, there are still residual errors after compensation, which will lead to channel phase perturbations [22]. Let the channel phase errors caused by residual propagation delay be $\boldsymbol{e}_\theta = [\boldsymbol{e}_{\theta_1}, \boldsymbol{e}_{\theta_2}, \ldots, \boldsymbol{e}_{\theta_K}]^T, \boldsymbol{e}_{\theta_k} = [e_{\theta_{k,1}}, e_{\theta_{k,2}}, \ldots, e_{\theta_{k,M}}]^T$, which follow the distribution of real Gaussian, i.e., $\mathrm{e}_{\theta_k} \sim N\left(0, \sigma_{\theta_k}^2\right)$ [23], $\sigma_{\theta_i}^2$ represents the variance of channel phase errors.

C. ARRAY RESPONSE

The array response vector of the UPA in (2) can be expressed as [24]:

$$\boldsymbol{a}_{k,l} \triangleq \boldsymbol{a}_{k,l}^{x} \otimes \boldsymbol{a}_{k,l}^{y} = \boldsymbol{a}_x\left(\phi_{k,l}^{x}\right) \otimes \boldsymbol{a}_y\left(\phi_{k,l}^{y}\right) \in \mathbb{C}^{M\times 1} \tag{5}$$

$$\boldsymbol{a}_{k,l}^{x} \triangleq \boldsymbol{a}_x\left(\phi_{k,l}^{x}\right) = \frac{1}{\sqrt{M_X}}[1, \exp\{-j\pi\phi_{k,l}^{x}\}, \ldots, \exp\{-j\pi(M_X-1)\phi_{k,l}^{x}\}] \in \mathbb{C}^{M_X\times 1} \tag{6}$$

$$\boldsymbol{a}_{k,l}^{y} \triangleq \boldsymbol{a}_y\left(\phi_{k,l}^{y}\right) = \frac{1}{\sqrt{M_Y}}[1, \exp\{-j\pi\phi_{k,l}^{y}\}, \ldots, \exp\{-j\pi(M_Y-1)\phi_{k,l}^{y}\}] \in \mathbb{C}^{M_Y\times 1} \quad (7)$$

where $\otimes$ represents Kronecker product, $\phi_{k,l}^{x} = \sin(\varphi_{k,l})\cos(\gamma_{k,l})$, $\phi_{k,l}^{y} = \cos(\varphi_{k,l})$, $\varphi_{k,l}$, $\gamma_{k,l}$ represent the angles with respect to the x- and y-axes associated with the propagation path l of the kth user, respectively. The calculation of the azimuth ($\varphi_{k,l}$) and elevation ($\gamma_{k,l}$) angles can be given by the LEO satellite ephemeris information and terminal location information. According to the ephemeris information and terminal location information, we can obtain the LEO satellite position information $\boldsymbol{X}_{leo} \in \mathbb{R}^3$ and the terminal position information $\boldsymbol{X}_{ut} \in \mathbb{R}^3$, both measured from Earth's center. Then, the azimuth ($\varphi_{k,l}$) and elevation ($\gamma_{k,l}$) angles can be calculated by $\left(\frac{\boldsymbol{X}_{leo}-\boldsymbol{X}_{ut}}{\|\boldsymbol{X}_{leo}-\boldsymbol{X}_{ut}\|}\right)$. In the high mobility communication scene, according to the LEO satellite trajectory and the general law of terminal motion, we can calculate the spatial angle information of the next moment at insatnt t to avoid the expiration of the information.

In conclusion, the channel vector $\boldsymbol{h}_k(t,f)$ can be further expressed as:

$$\boldsymbol{h}_k(t,f) = g_k(t,f)\cdot\boldsymbol{a}(k,l)\cdot\exp\left\{j2\pi[tf_{k,l}^{leo} - f\tau_k^{\min}]\right\} \quad (8)$$

where $g_k(t,f)$ represents the downlink channel gain of the kth user, which can be expressed as

$$g_k(t,f), \sum_{l=1}^{L} g_{k,l}\left\{j2\pi[t(f_{k,l}-f_{k,l}^{leo}) - f(\tau_{k,l}-\tau_k^{\min})]\right\} \quad (9)$$

The statistical characteristic of $g_k(t,f)$ depends on the propagation environment, for the LEO satellite communication scenario, the link power loss mainly includes the free space path loss and the atmospheric absorption loss. The free space path loss LP_{fs} can be given by

$$LP_{fs} = 20(\log_{10}(d) + \log_{10}(f) + \log_{10}(\frac{4\pi}{c})) \quad (10)$$

where d represents the the traveled distance, c represents the speed of light. The atmospheric absorption loss LP_{at} can refer to the reference [42].

Because of line of sight (LoS) transmission in LEO satellite communication systems, $g_k(t,f)$ can be modeled by Rician fading [25]. Let the Rician factor be k_k and the power be $\mathrm{E}\left\{|g_k(t,f)|^2\right\} = \lambda_k$. Therefor, $g_k(t,f)$ follows the distribution of independently and identically real-valued Gaussian with mean $\sqrt{\frac{k_k\lambda_k}{2(k_k+1)}}$ and variance $\frac{\lambda_k}{2(k_k+1)}$.

Considering the influence of residual Doppler shift and residual propagation delay in the channel estimation, let the estimated channel vector be $\hat{\boldsymbol{h}}_k$ and the actual channel vector be $\boldsymbol{h}_k$. Then, we model the actual channel vector $\boldsymbol{h}_k$ as:

$$\boldsymbol{h}_k = \hat{\boldsymbol{h}}_k \odot \boldsymbol{q}_{\theta_k} \odot \boldsymbol{p}_{f_k} = diag(diag(\hat{\boldsymbol{h}}_k)\boldsymbol{q}_{\theta_k})\boldsymbol{p}_{f_k} \quad (11)$$

where $\odot$ represents Hadamard product, $\boldsymbol{p}_{f_k}$ represents the channel error vector caused by residual Doppler shift, $\boldsymbol{q}_{\theta_k}$ represents the channel error vector caused by residual propagation delay, which can be expressed as:

$$\boldsymbol{q}_{\theta_k} = \exp\{j\boldsymbol{e}_{\theta_k}\} \quad (12)$$

Then the actual channel phase of the kth user at t_1 can be expressed as:

$$\theta_k(t_1) = \theta_k(t_0) + e_{\theta_k} \quad (13)$$

where $\boldsymbol{\theta} = [\theta_1, \theta_2, \ldots, \theta_K]^T$ represent the channel phase components with the elements independently and uniformly distributed between 0 and 2π.

IV. PROBLEM FORMULATION

Aiming at maximizing the EE, we investigate the robust energy-efficient hybrid beamforming design for LEO satellite communication systems. The EE can be denoted as the ratio of system rate to total power consumption.

A. SYSTEM RATE

The SINR of the kth user in the system can be calculated according to (1), i.e.,

$$\mathrm{SINR}_k \triangleq \frac{\left|\boldsymbol{b}_k^H\boldsymbol{h}_k\right|^2}{\sum_{i\neq k}\left|\boldsymbol{b}_i^H\boldsymbol{h}_k\right|^2 + N_0}, \quad \forall k \in K \quad (14)$$

According to the analysis of the channel model in the previous section, the actual CSI of the LEO satellite communication system is a constantly changing random process, and it is not feasible to obtain the instantaneous and accurate CSI. To this end, we adopt the statistics averaging method for the system rate modelling [26], and the ergodic capacity of the LEO satellite communication system can be expressed as:

$$\begin{aligned} R &\triangleq \sum_{k=1}^{K}\int_0^{\infty} B\log_2(1+\mathrm{SINR}_k)P(\mathrm{SINR}_k)d(\mathrm{SINR}_k) \\ &= \sum_{k=1}^{K} E[B\log_2(1+\mathrm{SINR}_k)] \end{aligned} \quad (15)$$

where B represents the channel bandwidth, and $P(\mathrm{SINR}_k)$ represents the probability of SINR_k.

B. SYSTEM POWER CONSUMPTION

The power consumption of the LEO satellite communication system includes transmit power consumption and circuit hardware power consumption. The total power consumption can be expressed as:

$$P_{total} \triangleq \sum_{k=1}^{K}\|\boldsymbol{b}_k\|_2^2 + P_0 \quad (16)$$

where the first term is the power of the kth user radiated by the transmitting antennas, which should meet the transmit power constraint of the LEO satellite communication system, i.e.,

$$\sum_{k=1}^{K}\|\boldsymbol{b}_k\|^2 \leq P_T \quad (17)$$

The second term P_0 represents the power consumption of circuit hardware, such as the transmitting antennas in the LEO satellite communication system. In this paper, the LEO satellite transmitter adopts a hybrid beamforming architecture based on full connection, and each user terminal is configured with a single antenna. Thus, P_0 can be expressed as [27]:

$$P_0 = P_t + KP_r + P_{syn} \tag{18}$$

$$P_t = N_{RF}MP_{ps} + N_{RF}R_{RFC} + P_{LO} + P_{BB} \tag{19}$$

$$P_{RFC} = P_{ADC} + P_{mixer} + P_{LPF} + P_{BBA} \tag{20}$$

$$P_r = P_{RFC} + P_{LO} + P_{BB} \tag{21}$$

where P_t represents the power consumption of the LEO satellite's antenna array, P_r represents the power consumption of the user's antenna, and P_{syn} represents the basic power consumption of the LEO satellite, $P_{PS}, P_{LO}, P_{BBA}, P_{DAC}, P_{mixer}, P_{LPF}, P_{BBA}$ represent the power consumption of phase shifter, local oscillator, precoder, digital to analog converter, mixer, low-pass filter, and baseband amplifier, respectively.

C. PROBLEM MODELING

In conclusion, the system EE can be defined as:

$$\mathrm{EE} \triangleq \frac{R}{P_{total}} = \frac{\sum_{k=1}^{K} E[B\log_2(1+\mathrm{SINR}_k)]}{\sum_{k=1}^{K}\|\boldsymbol{b}_k\|_2^2 + P_0} \quad \text{(bits/Joule)} \tag{22}$$

Considering the constraints of transmit power and QoS, and taking EE maximization as the optimization goal, the optimization problem can be modeled as:

$$Q_1: \quad \max_{\{\boldsymbol{b}_k\}_1^K} \mathbf{EE} = \frac{B\sum_{k=1}^{K} E\left\{\log_2\left(1+\frac{|\boldsymbol{b}_k^H\boldsymbol{h}_k|^2}{\sum_{i\neq k}|\boldsymbol{b}_i^H\boldsymbol{h}_k|^2+N_0}\right)\right\}}{\sum_{k=1}^{K}\|\boldsymbol{b}_k\|_2^2 + P_0} \tag{23}$$

$$s.t.\ E\{\mathrm{SINR}_k\} \geq r_k, \quad \forall k \in [1,2,\ldots,K], \tag{24}$$

$$\sum_{k=1}^{K}\|\boldsymbol{b}_k\|_2^2 \leq P_T. \tag{25}$$

where r_k represents the SINR constraint threshold of the kth user.

V. ROBUST HYBRID BEAMFORMING DESIGN

It is worth noting that the ergodic user rate and ergodic SINR would not allow explicit expressions, to handle this challenge, we invoke the explicit tight approximations of them. To simplify problem Q_1, we adopt SDP algorithm to transform the optimization problem equivalently. We can observe that optimization problem is a general nonconvex sum-of-ratios fractional programming problem, to this end, we propose an inner and outer nested iterative algorithm combining QTFP and CCCP. In addition, it is worth noting that there is a rank-one constraint in SDP algorithm, which can be handled by adopting the penalty function algorithm. Finally, we adopt low complexity NFDM algorithm and AltOpt algorithm to jointly solve digital beamforming matrix and analog beamforming matrix.

A. APPROXIMATED ERGODIC USER RATE AND ERGODIC SINR

We can observe that both the ergodic user rate and the ergodic SINR in (15) and (14) do not admit explicit expressions, to handle this problem, some researches use Monte Carlo method [28] for statistical simulation, which might be not practical due to the high computational complexity and huge demand for storage memory. To handle this challenge, we invoke the approximation $\bar{R}_k$ of ergodic user rate and the approximation $\overline{\mathrm{SINR}}_k$ of ergodic SINR as follows [29]:

$$R_k \approx \bar{R}_k \triangleq \log_2\left(1+\frac{E\left\{\left|\boldsymbol{b}_k^H\boldsymbol{h}_k\right|^2\right\}}{E\left\{\sum_{i\neq k}\left|\boldsymbol{b}_i^H\boldsymbol{h}_k\right|^2\right\}+N_0}\right) \tag{26}$$

$$\mathrm{SINR}_k \approx \overline{\mathrm{SINR}}_k \triangleq \frac{E\left\{\left|\boldsymbol{b}_k^H\boldsymbol{h}_k\right|^2\right\}}{E\left\{\sum_{i\neq k}\left|\boldsymbol{b}_i^H\boldsymbol{h}_k\right|^2\right\}+N_0} \tag{27}$$

It should be noted that the approximations in (26) and (27) are both very tight and have been theoretically analyzed and numerically verified in previous works [29].

B. SDP ALGORITHM

We can observe that the objective function and constraints (24), (25) in problem Q_1 involve the second power of $\boldsymbol{b}_k$, thus, problem Q_1 is a typical nonconvex quadratic constrained quadratic programming (QCQP) problem [30]. To handle this challenge, we adopt the SDP algorithm [31], and then transform the optimization variables $\{\boldsymbol{b}_k\}_{k=1}^K$ into $\left\{\boldsymbol{W}_k \triangleq \boldsymbol{b}_k\boldsymbol{b}_k^H\right\}_{k=1}^K$, the new variable $\boldsymbol{W}_k$ should satisfy the constraints of $\boldsymbol{W}_k \succ 0$ and $\mathrm{rank}(\boldsymbol{W}_k) = 1$. Then, the approximation ergodic user rate $\bar{R}_k$ in (26) can be written as:

$$\begin{aligned}\bar{R}_k &= B\log_2\left(1+\frac{E\{\mathrm{Tr}(\boldsymbol{H}_k\boldsymbol{W}_k)\}}{E\left\{\sum_{i\neq k}\mathrm{Tr}(\boldsymbol{H}_k\boldsymbol{W}_i)\right\}+N_0}\right)\\ &= B\log_2\left(1+\frac{\mathrm{Tr}(E\{\boldsymbol{H}_k\boldsymbol{W}_k\})}{\sum_{i\neq k}\mathrm{Tr}(E\{\boldsymbol{H}_k\boldsymbol{W}_i\})+N_0}\right)\\ &= B\log_2\left(1+\frac{\mathrm{Tr}(\bar{\boldsymbol{H}}_k\boldsymbol{W}_k)}{\sum_{i\neq k}\mathrm{Tr}(\bar{\boldsymbol{H}}_k\boldsymbol{W}_i)+N_0}\right)\end{aligned} \tag{28}$$

where $\boldsymbol{H}_k \in \mathbb{C}^{M\times M}$ denotes the instantaneous channel correlation matrix of the kth user and $\bar{\boldsymbol{H}}_k \in \mathbb{C}^{M\times M}$ represents the long term channel correlation matrix of the kth user, as follows:

$$\bar{\boldsymbol{H}}_k = E\{\boldsymbol{H}_k\} \triangleq E\{\boldsymbol{h}_k\boldsymbol{h}_k^H\} = \mathrm{diag}(\hat{\boldsymbol{h}}_k)\boldsymbol{Q}_{\theta_k}\boldsymbol{P}_{f_k}\mathrm{diag}(\hat{\boldsymbol{h}}_k^H) \tag{29}$$

where $\boldsymbol{Q}_{\theta_k}$ represents the expectation of the autocorrelation matrix of the channel error vector $\boldsymbol{q}_{\theta_k}$ caused by the residual propagation delay, $\boldsymbol{P}_{f_k}$ represents the expectation of the autocorrelation matrix of the channel error vector $\boldsymbol{p}_{f_k}$ caused by the residual Doppler shift. $\boldsymbol{Q}_{\theta_k}$ can be written as:

$$\begin{aligned}\boldsymbol{Q}_{\theta_k} &= E\left\{\boldsymbol{q}_{\theta_k}\boldsymbol{q}_{\theta_k}^H\right\} \\ &= E\left\{[e^{je_{k,1}}, e^{je_{k,2}}, \ldots, e^{je_{k,M}}]^T[e^{je_{k,1}}, e^{je_{k,2}}, \ldots, e^{je_{k,M}}]\right\} \\ &= E\left\{\begin{array}{ccc} 1 & \cdots & e^{je_{k,1}}e^{-je_{k,M}} \\ \vdots & \ddots & \vdots \\ e^{je_{k,M}}e^{-je_{k,1}} & \cdots & 1 \end{array}\right\} \\ &= \left\{\begin{array}{ccc} 1 & \cdots & E\left\{e^{je_{k,1}}e^{-je_{k,M}}\right\} \\ \vdots & \ddots & \vdots \\ E\left\{e^{je_{k,M}}e^{-je_{k,1}}\right\} & \cdots & 1 \end{array}\right\}\end{aligned} \tag{30}$$

It can be observed that the diagonal elements in $\boldsymbol{Q}_{\theta_k}$ are all one, the elements in row m and column n on the non diagonal line can be written as $E\left\{e^{je_{k,m}}e^{-je_{k,n}}\right\} = E\left\{e^{je_{k,m}}\right\}E\left\{e^{-je_{k,n}}\right\}$.

$$\begin{aligned}E\left\{e^{je_{k,m}}\right\} &= \int_{-\infty}^{\infty} e^{j\bar{e}}\frac{1}{\sqrt{2\pi}\sigma_{\theta_k}}e^{-\frac{\bar{e}^2}{2\sigma_{\theta_k}^2}}d\bar{e} \\ &= e^{-\frac{\sigma_{\theta_k}^2}{2}}\int_{-\infty}^{\infty}\frac{1}{\sqrt{2\pi}\sigma_{\theta_k}}e^{-\frac{\left(\bar{e}-j\sigma_{\theta_k}\right)^2}{2\sigma_{\theta_k}^2}}d\bar{e} = e^{-\frac{\sigma_{\theta_k}^2}{2}}\end{aligned} \tag{31}$$

Thus, the elements in matrix $\boldsymbol{Q}_{\theta_k}$ can be given by

$$\left[\boldsymbol{Q}_{\theta_k}\right]_{m,n} = \begin{cases} 1, & m = n \\ e^{-\sigma_{\theta_k}^2}, & m \neq n \end{cases} \tag{32}$$

Besides, $\boldsymbol{p}_{f_k}$ follows the distribution of *Jacks*, and its autocorrelation matrix $\boldsymbol{P}_{f_k}$ can be expressed as:

$$\boldsymbol{P}_{f_k} = E\{\boldsymbol{p}_{f_k}\boldsymbol{p}_{f_k}^H\} = J_0(2\pi f \mathrm{V}T) \tag{33}$$

where f represents the carrier frequency, $\mathrm{V}T$ represents the sum of the round-trip delay of the communication link and the duration of the communication frame.

In conclusion, Q_1 can be equivalently transformed into

$$Q_2: \quad \max_{\{\boldsymbol{W}_k\}_1^K} \frac{B\sum_{k=1}^{K}\log_2\left(1+\frac{\mathrm{Tr}(\bar{\boldsymbol{H}}_k\boldsymbol{W}_k)}{\sum_{i\neq k}\mathrm{Tr}(\bar{\boldsymbol{H}}_k\boldsymbol{W}_i)+N_0}\right)}{\sum_{k=1}^{K}\mathrm{Tr}\left(\boldsymbol{W}_k\right)+P_0} \tag{34}$$

$$s.t.\ \mathrm{Tr}\left(\bar{\boldsymbol{H}}_k\boldsymbol{W}_k\right) \geq r_k\left(\sum_{i\neq k}\mathrm{Tr}\left(\bar{\boldsymbol{H}}_k\boldsymbol{W}_i\right)+N_0\right) \tag{35}$$

$$\sum_{i=1}^{K}\mathrm{Tr}\left(\boldsymbol{W}_k\right) \leq P_T \tag{36}$$

$$\boldsymbol{W}_k \succ 0, \quad \forall k \in [1, 2, \ldots, K] \tag{37}$$

$$\mathrm{rank}(\boldsymbol{W}_k) = 1 \tag{38}$$

To facilitate analysis, we equivalently transform the denominator term in (34), Q_2 can be equivalently transformed into (39), as shown at the bottom of the page.

C. QTFP ALGORITHM

We can observe that Q_3 is a sum-of-ratios fractional programming problem, to this end, we adopt the quadratic transformation method. According to the quadratic transformation theory [32], problem Q_3 is equivalent to

$$\begin{aligned}Q_4: \quad \max_{\{\boldsymbol{W}_k\}_1^K} \; & B\left(2y\left(\sum_{k=1}^{K}\left(\mathbf{U}_k\left(\boldsymbol{W}\right)-\mathbf{V}_k\left(\boldsymbol{W}\right)\right)\right)^{1/2}\right. \\ & \left. - y^2\left(\sum_{k=1}^{K}\mathrm{Tr}\left(\boldsymbol{W}_k\right)+P_0\right)\right) \\ s.t.\ & (35),(36),(37),(38)\end{aligned} \tag{40}$$

where y is the introduced auxiliary variable, and $U_k\left(\mathbf{W}\right)$ and $V_k\left(\mathbf{W}\right)$ are the introduced auxiliary functions as follows:

$$U_k\left(\boldsymbol{W}\right) = \log_2\left(\mathrm{Tr}\left(\sum_{k=1}^{K}\bar{\boldsymbol{H}}_k\boldsymbol{W}_k\right)+N_0\right) \tag{41}$$

$$V_k\left(\boldsymbol{W}\right) = \log_2\left(\mathrm{Tr}\left(\sum_{i\neq k}\bar{\boldsymbol{H}}_k\boldsymbol{W}_i\right)+N_0\right) \tag{42}$$

$$y^{(\tau)} = \frac{\sqrt{B\left(U_k\left(\boldsymbol{W}^{(\tau)}\right)-V_k\left(\boldsymbol{W}^{(\tau)}\right)\right)}}{\sum_{k=1}^{K}\mathrm{Tr}\left(\boldsymbol{W}_k^{(\tau)}\right)+P_0} \tag{43}$$

where τ represents the iteration index. During optimization, we optimize the original variables $\boldsymbol{W} = \{\boldsymbol{W}_1, \boldsymbol{W}_2, \ldots, \boldsymbol{W}_K\}$ by updating the auxiliary variable y iteratively.

D. CCCP ALGORITHM

We can observe from (41) and (42) that $U_k\left(\boldsymbol{W}\right)$ and $V_k\left(\boldsymbol{W}\right)$ are both concave functions of $\boldsymbol{W}$, so Q_3 is a difference of convex (DC) programming [33]. To handle this challenge, we invoke the CCCP algorithm to address this DC programming. The CCCP algorithm is a monotonically decreasing

$$\begin{aligned}Q_3: \quad \max_{\{\boldsymbol{W}_k\}_1^K} \; & \frac{B\sum_{k=1}^{K}\left(\log_2\left(\mathrm{Tr}\left(\sum_{k=1}^{K}\bar{\boldsymbol{H}}_k\boldsymbol{W}_k\right)+N_0\right)-\log_2\left(\mathrm{Tr}\left(\sum_{i\neq k}\bar{\boldsymbol{H}}_k\boldsymbol{W}_i\right)+N_0\right)\right)}{\sum_{k=1}^{K}\mathrm{Tr}\left(\boldsymbol{W}_k\right)+P_0} \\ s.t.\ & (35),(36),(37),(38)\end{aligned} \tag{39}$$

global optimization method, which can be used to solve nonconvex optimization problems [34]. The basic idea is to replace $V_k(\boldsymbol{W})$ in (42) with its first-order Taylor expansion $V_k^{te}(\boldsymbol{W})$ at the current iteration firstly, according to the properties of the Taylor expansion, $V_k^{te}(\boldsymbol{W})$ is the upper bound of $V_k(\boldsymbol{W})$, i.e., $V_k(\boldsymbol{W}) \leq V_k^{te}(\boldsymbol{W})$. Then, we solve this convex optimization problem with an initial feasible point, and continue to the next iteration. Thus, problem Q_4 can be transformed into

$$Q_5: \max_{\{\boldsymbol{W}_k\}_1^K} B\left(2y\left(\sum_{k=1}^{K}\left(\mathrm{U}_k(\boldsymbol{W}) - \mathrm{V}_k^{te,(\mu)}(\boldsymbol{W})\right)\right)^{1/2} - y^2\left(\sum_{k=1}^{K}\mathrm{Tr}(\boldsymbol{W}_k) + P_0\right)\right)$$
$$s.t.\ (35),(36),(37),(38) \tag{44}$$

where τ represents the iteration index, the first-order Taylor expansion V_k^{te} (W) in the iteration can be expressed as:

$$\mathrm{V}_k^{te,(\mu)}(\boldsymbol{W}) = \mathrm{V}_k\left(\boldsymbol{W}^{(\mu)}\right) + \sum\nolimits_{i\neq k}\mathrm{Tr}\left\{\left(\frac{\partial V_k\left(\boldsymbol{W}^{(\mu)}\right)}{\partial \boldsymbol{W}_i}\right)^T\left(\boldsymbol{W}_i - \boldsymbol{W}_i^{(\mu)}\right)\right\} \tag{45}$$

$$\frac{\partial \mathrm{V}_k\left(\boldsymbol{W}^{(\mu)}\right)}{\partial \boldsymbol{W}_i} = \frac{\left(\bar{\boldsymbol{H}}_k\right)^T}{\ln 2\cdot\left(\mathrm{Tr}\left(\sum_{i\neq k}\bar{\boldsymbol{H}}_k\boldsymbol{W}_i^{(\mu)}\right) + N_0\right)} \tag{46}$$

After transformation, the objective function in problem Q_5 is transformed into a concave function, which can be solved by convex optimization method. The basic idea is to initialize the feasible solution $\boldsymbol{W}^{(\mu=0)}$, use the auxiliary variable y in the iteration, and bring it into Q_5 for iterative solution, until the convergence condition or the maximum number of iterations is reached.

E. PENALTY FUNCTION ALGORITHM

1) ALGORITHM APPLICATION ANALYSIS

It is worth noting that there is a rank-one constraint in problem Q_5, to solve this problem, some references adopt semidefinite relaxation (SDR) algorithm [35], which directly removes the rank-one constraint. Then, based on the obtained optimization variables, this algorithm randomly generates a hybrid beamforming matrix pool satisfying the rank-one constraint by Gaussian randomization method or eigenvalue decomposition method, and selects the local optimum as the approximate solution. However, the performance of the approximate solution of SDR algorithm may be far worse than that of the optimal solution, especially under the high-dimensional matrix. To handle this challenge, we invoke the penalty function algorithm [43], [44].

Motivated by the fact that $\mathrm{rank}(\boldsymbol{W}_k) = 1 \Leftrightarrow \mathrm{Tr}(\boldsymbol{W}_k) - \lambda_{\max}(\boldsymbol{W}_k) = 0$, we adopt the nonsmooth method to convert the rank-one constraint (38) to

$$\mathrm{Tr}(\boldsymbol{W}_k) - \lambda_{\max}(\boldsymbol{W}_k) \leq 0 \tag{47}$$

where $\lambda_{\max}(\boldsymbol{W}_k)$ represents the maximum eigenvalue of matrix $\boldsymbol{W}_k$. For any $\boldsymbol{W}_k \succeq 0$, we note that $\mathrm{Tr}(\boldsymbol{W}_k) - \lambda_{\max}(\boldsymbol{W}_k) \geq 0$ always holds true. Therefor, (47) is equivalent to $\mathrm{Tr}(\boldsymbol{W}_k) - \lambda_{\max}(\boldsymbol{W}_k) = 0$. It means that matrix $\boldsymbol{W}_k$ has only one nonzero eigenvalue, i.e.,

$$\boldsymbol{W}_k = \lambda_{\max}(\boldsymbol{W}_k)\boldsymbol{w}_{k,\max}\boldsymbol{w}_{k,\max}^H \tag{48}$$

where $\boldsymbol{w}_{k,\max}$ is the unit eigenvector corresponding to the maximum eigenvalue $\lambda_{\max}(\boldsymbol{W}_k)$. Thus, problem Q_5 can be transformed into

$$Q_6: \max_{\{\boldsymbol{W}_k\}_1^K} B\left(2y\left(\sum_{k=1}^{K}\left(\mathrm{U}_k(\boldsymbol{W}) - \mathrm{V}_k^{te,(\mu)}(\boldsymbol{W})\right)\right)^{1/2} - y^2\left(\sum_{k=1}^{K}\mathrm{Tr}(\boldsymbol{W}_k) + P_0\right)\right)$$
$$s.t.\ (35),\ (36),(37),(47) \tag{49}$$

It is essential to point out that if $\mathrm{Tr}(\boldsymbol{W}_k) - \lambda_{\max}(\boldsymbol{W}_k)$ is small enough, the matrix $\boldsymbol{W}_k$ can be approximated to $\lambda_{\max}(\boldsymbol{W}_k)\boldsymbol{w}_{k,\max}\boldsymbol{w}_{k,\max}^H$, i.e. $\boldsymbol{W}_k \approx \lambda_{\max}(\boldsymbol{W}_k)\boldsymbol{w}_{k,\max}\boldsymbol{w}_{k,\max}^H$. If the error meets the established accuracy requirement, we can think that the matrix $\boldsymbol{W}_k$ satisfies the rank-one condition. Therefor, to achieve this goal, our main work is to make $\mathrm{Tr}(\boldsymbol{W}_k) - \lambda_{\max}(\boldsymbol{W}_k)$ as small as possible. To tackle this difficulty, we exploit the penalty function algorithm to incorporate the constraint (47) into the objective function. Then, problem Q_6 can be transformed into

$$Q_7: \max_{\{\boldsymbol{W}_k\}_1^K} B\left(2y\left(\sum_{k=1}^{K}\left(\mathrm{U}_k(\boldsymbol{W}) - \mathrm{V}_k^{te,(\mu)}(\boldsymbol{W})\right)\right)^{1/2} - y^2\left(\sum_{k=1}^{K}\mathrm{Tr}(\boldsymbol{W}_k) + P_0\right)\right) - \xi\sum_{k=1}^{K}\left(\mathrm{Tr}(\boldsymbol{W}_k) - \lambda_{\max}(\boldsymbol{W}_k)\right)$$
$$s.t.\ (35),\ (36),(37) \tag{50}$$

where ξ is a penalty factor large enough to obtain small value of $\mathrm{Tr}(\boldsymbol{W}_k) - \lambda_{\max}(\boldsymbol{W}_k)$. Clearly, the problem Q_7 is to maximize the original objective function (49) and minimize the value of $\mathrm{Tr}(\boldsymbol{W}_k) - \lambda_{\max}(\boldsymbol{W}_k)$. By setting the reasonable initial penalty factor ξ and feasible solution $\left\{\boldsymbol{W}_k^{(0)}\right\}_{k=1}^K$, we can obtain that $\mathrm{Tr}(\boldsymbol{W}_k) - \lambda_{\max}(\boldsymbol{W}_k) \approx 0$ after repeated iterative calculation, which means that $\boldsymbol{W}_k$ has only one non-zero eigenvalue, and the rank-one constraint (38) is satisfied [45].

It is worth noting that $\mathrm{Tr}(\boldsymbol{W}_k)$ is a linear function of $\boldsymbol{W}_k$, and $\lambda_{\max}(\boldsymbol{W}_k)$ is convex in $\boldsymbol{W}_k$. $\mathrm{Tr}(\boldsymbol{W}_k) - \lambda_{\max}(\boldsymbol{W}_k)$ is convex in $\boldsymbol{W}_k$. Meanwhile, the function $\lambda_{\max}(\boldsymbol{W}_k)$ is nonsmooth, which may lead to the non-convexity of the problem Q_7. To this end, we replace $\lambda_{\max}(\boldsymbol{X})$ in (50) with its first-order Taylor expansion $\lambda_{\max}^{te}(\boldsymbol{W}_k)$ at the current iteration.

The sub-gradient property of $\lambda_{\max}(\boldsymbol{X})$ can be expressed as $\frac{\partial \lambda_{\max}(\boldsymbol{W}_k)}{\partial \boldsymbol{W}_k} = \boldsymbol{w}_{k,\max}\boldsymbol{w}_{k,\max}^H$, so we have

$$\lambda_{\max}(\boldsymbol{W}_k) \geq \lambda_{\max}(\boldsymbol{W}_{k,0}) + \left\langle \boldsymbol{w}_{k,\max}\boldsymbol{w}_{k,\max}^H, \boldsymbol{W}_k - \boldsymbol{W}_{k,0} \right\rangle, \quad \forall \boldsymbol{W}_k \succ 0 \tag{51}$$

where $\langle \boldsymbol{A}, \boldsymbol{B} \rangle = \mathrm{Tr}(\boldsymbol{A}^H\boldsymbol{B})$.

Then, substituting the transformation in (51) into problem Q_7 to relax the function $\lambda_{\max}(\boldsymbol{W}_k)$, we can get the optimization problem as follows

$$\begin{aligned} Q_8: \quad \max_{\{\boldsymbol{W}_k\}_1^K} \; & B\left(2y\left(\sum_{k=1}^{K}\left(\mathrm{U}_k(\boldsymbol{W}) - \mathrm{V}_k^{te,(\mu)}(\boldsymbol{W})\right)\right)^{1/2} \right. \\ & - y^2\left(\sum_{k=1}^{K}\mathrm{Tr}(\boldsymbol{W}_k) + P_0\right)\Bigg) \\ & - \xi\sum_{k=1}^{K}\left(\mathrm{Tr}(\boldsymbol{W}_k) - \lambda_{\max}\left(\boldsymbol{W}_k^{(\mu)}\right)\right. \\ & \left. - \left\langle \boldsymbol{w}_{k,\max}^{(\mu)}\boldsymbol{w}_{k,\max}^{(\mu)H}, \boldsymbol{W}_k - \boldsymbol{W}_k^{(\mu)} \right\rangle\right) \\ s.t. \; & (35), (36), (37) \end{aligned} \tag{52}$$

where $\boldsymbol{W}_k^{(\mu)}$ is the solution of problem Q_8 obtained in the μth iteration.

2) ALGORITHM CONVERGENCE ANALYSIS

To ensure the effectiveness of the penalty function algorithm, we analyze the convergence of the algorithm. Let the optimal solution of problem Q_8 after the μth iteration be $\boldsymbol{W}^{(\mu+1)}$ and the value of the objective function be $\mathrm{F}\left(\boldsymbol{W}^{(\mu+1)}\right)$, we can obtain:

$$\begin{aligned} & \mathrm{F}\left(\boldsymbol{W}^{(\mu+1)}\right) \\ = \; & B\left(2y\left(\sum_{k=1}^{K}\left(\mathrm{U}_k\left(\boldsymbol{W}^{(\mu+1)}\right) - \mathrm{V}_k^{te,(\mu+1)}\left(\boldsymbol{W}^{(\mu+1)}\right)\right)\right)^{1/2} \right. \\ & - y^2\left(\sum_{k=1}^{K}\mathrm{Tr}\left(\boldsymbol{W}_k^{(\mu+1)}\right) + P_0\right)\Bigg) - \xi\sum_{k=1}^{K}\left(\mathrm{Tr}\left(\boldsymbol{W}_k^{(\mu+1)}\right)\right. \\ & \left. - \lambda_{\max}\left(\boldsymbol{W}_k^{(\mu+1)}\right)\right) \\ \geq \; & B\left(2y\left(\sum_{k=1}^{K}\left(\mathrm{U}_k\left(\boldsymbol{W}^{(\mu+1)}\right) - \mathrm{V}_k^{te,(\mu+1)}\left(\boldsymbol{W}^{(\mu+1)}\right)\right)\right)^{1/2} \right. \\ & - y^2\left(\sum_{k=1}^{K}\mathrm{Tr}\left(\boldsymbol{W}_k^{(\mu+1)}\right) + P_0\right)\Bigg) \\ & - \xi\sum_{k=1}^{K}\left(\mathrm{Tr}\left(\boldsymbol{W}_k^{(\mu+1)}\right) - \lambda_{\max}\left(\boldsymbol{W}_k^{(\mu)}\right)\right. \\ & \left. - \left\langle \boldsymbol{w}_{k,\max}^{(\mu)}\boldsymbol{w}_{k,\max}^{(\mu)H}, \boldsymbol{W}_k^{(\mu+1)} - \boldsymbol{W}_k^{\mu} \right\rangle\right) \end{aligned}$$

$$\begin{aligned} \overset{by(47)}{\geq} \; & B\left(2y\left(\sum_{k=1}^{K}\left(U_k\left(\boldsymbol{W}^{(\mu)}\right) - V_k^{te,(\mu)}\left(\boldsymbol{W}^{(\mu)}\right)\right)\right)^{1/2} \right. \\ & - y^2\left(\sum_{k=1}^{K}\mathrm{Tr}\left(\boldsymbol{W}_k^{\mu}\right) + P_0\right)\Bigg) - \xi\sum_{k=1}^{K}\left(\mathrm{Tr}\left(\boldsymbol{W}_k^{(\mu)}\right)\right. \\ & \left. - \lambda_{\max}\left(\boldsymbol{W}_k^{(\mu)}\right)\right) \\ = \; & \mathrm{F}\left(\boldsymbol{W}^{(\mu)}\right) \end{aligned} \tag{53}$$

which demonstrates the effectiveness of iterative penalty function algorithm.

Therefor, by giving the reasonable initial penalty factor ξ and feasible solution $\left\{\boldsymbol{W}_k^{(0)}\right\}_{k=1}^K$, we can iterate a convergent result $\left\{\boldsymbol{W}_k^{(\mu)}\right\}_{k=1}^K$ as an improved solution of (49) through solving (52).

In conclusion, the optimization algorithm of variables $\{\boldsymbol{W}\}_{k=1}^K$ can be decomposed into two-layer nested iterations and then solved alternately, which can be described as follows:

Algorithm Outer Iterative Algorithm

Input: Initial feasible positive semidefinite matrices $\left\{\boldsymbol{W}_k^{(\tau=0)}\right\}_{k=1}^K$, outer iteration index $\tau = 0$, threshold $\varepsilon_1 = 10^{-3}$, energy efficiency $EE^{(\tau)}$.

1. **Repeat**
2. For fixed $\left\{\boldsymbol{W}_k^{(\tau)}\right\}_{k=1}^K$, update $y^{(\tau)}$ by (43).
3. For fixed $y^{(\tau)}$, substituting $y^{(\tau)}$ into (52), obtain the solutions $\left\{\boldsymbol{W}_{opt}^{(\mu_{end})}\right\}_{k=1}^K$ by inner iterative algorithm.
4. Update $\left\{\boldsymbol{W}_k^{(\tau+1)}\right\}_{k=1}^K = \left\{\boldsymbol{W}_{opt}^{(\mu_{end})}\right\}_{k=1}^K$, set $\tau = \tau + 1$.
5. Calculate $EE^{(\tau+1)}$ by (43).
6. **Until** $\left|EE^{(\tau+1)} - EE^{(\tau)}\right| \leq \varepsilon_1$.
7. Obtain the solutions $\{\boldsymbol{W}_{opt}\}_{k=1}^K = \left\{\boldsymbol{W}_k^{\tau_{end}}\right\}_{k=1}^K$.

Output: $\{\boldsymbol{W}_{opt}\}_{k=1}^K$.

F. JOINT DESIGN ALGORITHM OF DIGITAL BEAMFORMING MATRIX AND ANALOG BEAMFORMING MATRIX

In this paper, the final optimization solutions we need to obtain are the digital beamforming matrix and the analog beamforming matrix in the hybrid beamformer, we have obtained the optimization variables $\{\boldsymbol{W}_{opt}\}_{k=1}^K$ through the calculation in the previous section. In this section, we need to recover the hybrid beamforming matrix $\boldsymbol{B}_{opt}^*$ from $\{\boldsymbol{W}_{opt}\}_{k=1}^K$. Then, the digital beamforming matrix $\boldsymbol{W}_{BB}$ and the analog beamforming matrix $\boldsymbol{W}_{RF}$ can be obtained based on the $\boldsymbol{B}_{opt}^*$. In conclusion, the optimization algorithm of variables $\boldsymbol{W}_{BB}$ and $\boldsymbol{W}_{RF}$ can be decomposed into two phases, which can be described as follows:

Algorithm Inner Iterative Algorithm

Input: Inner iteration index μ, penalty iteration index m, thresholds $\varepsilon_2 = 10^{-3}, \varepsilon_3 = 10^{-3}$ penalty factor $\xi = 2$, energy efficiency $EE^{(\mu)}$.

1. **Repeat**
   Initial feasible positive semidefinite matrices $\left\{\boldsymbol{W}_k^{(\mu=0)}\right\}_{k=1}^K = \left\{\boldsymbol{W}_k^{(\tau=0)}\right\}_{k=1}^K$ and $y^{(\mu)}$.
2. **Repeat**
3. Initial feasible positive semidefinite matrices $\left\{\boldsymbol{W}_k^{(m=0)}\right\}_{k=1}^K = \left\{\boldsymbol{W}_k^{(u=0)}\right\}_{k=1}^K$
4. Calculate the maximum eigenvalue $\lambda_{\max}\left(\boldsymbol{W}_k^{(m)}\right)$ of each $\boldsymbol{W}_k^{(m)}$ and the corresponding eigenvector $\boldsymbol{w}_{k,\max}^{(m)}$.
5. Obtain the solutions $\left\{\boldsymbol{W}_k'\right\}_{k=1}^K$ by (52) based on convex optimization method.
6. Update $\left\{\boldsymbol{W}_k^{(m+1)}\right\}_{k=1}^K = \left\{\boldsymbol{W}_k'\right\}_{k=1}^K$.
7. if $\left\{\boldsymbol{W}_k^{(m+1)}\right\}_{k=1}^K \approx \left\{\boldsymbol{W}_k^{(m)}\right\}_{k=1}^K$, then
8. set $\xi = 2\xi$;
9. else
10. set $m = m + 1$;
11. end.
12. **Until** $\left|\mathrm{Tr}\left(\boldsymbol{W}_k^{(m)}\right) - \lambda_{\max}\left(\boldsymbol{W}_k^{(m)}\right)\right| \le \varepsilon_3$.
13. Calculate $EE^{(\mu+1)}$ by (43), set $\mu = \mu + 1$.
14. **Until** $\left|EE^{(\mu+1)} - EE^{(\mu)}\right| \le \varepsilon_2$.
15. Obtain the solutions $\left\{\boldsymbol{W}_{opt}^{(\mu_{end})}\right\}_{k=1}^K$.

Output: $\left\{\boldsymbol{W}_{opt}^{(\mu_{end})}\right\}_{k=1}^K$.

1) DESIGN OF HYBRID BEAMFORMING MATRIX $\boldsymbol{B}_{opt}^*$

To obtain $\boldsymbol{B}_{opt}^*$, we adopt the eigenvalue decomposition (EVD) algorithm [36], which can be formulated as:

$$\min_{\boldsymbol{b}_k} \left\| \boldsymbol{W}_{k,opt} - \boldsymbol{b}_k \boldsymbol{b}_k^H \right\|_F^2 \tag{54}$$

where the optimal solution $\boldsymbol{b}_k^*$ can be given by multiplying the maximum eigenvector of $\boldsymbol{W}_{k,opt}$ by the root of the maximum eigenvalue, the maximum eigenvector and maximum eigenvalue can be obtained by EVD algorithm. Then, we can obtain the hybrid beamforming vectors of K users, i.e., $\boldsymbol{B}_{opt}^* = \left\{\boldsymbol{b}_k^*\right\}_{k=1}^K$.

2) JOINT DESIGN OF DIGITAL BEAMFORMING MATRIX $\boldsymbol{W}_{BB}$ AND ANALOG BEAMFORMING MATRIX $\boldsymbol{W}_{RF}$

In this phase, we need to calculate the digital beamforming matrix $\boldsymbol{W}_{BB}$ and the analog beamforming matrix $\boldsymbol{W}_{RF}$ based on $\boldsymbol{B}_{opt}^*$. We can observe that this problem is a joint optimization problem of two matrix variables, which can be regarded as a matrix decomposition problem with power and constant modulus constraints. To handle this problem, we invoke the low complexity algorithms, i.e., NFDM algorithm and AltOpt algorithm [37], which can be formulated as:

$$P_1: \quad \min_{\boldsymbol{W}_{RF}\boldsymbol{W}_{BB}} \left\| \boldsymbol{B}_{opt}^* - \boldsymbol{W}_{RF}\boldsymbol{W}_{BB} \right\|_F \tag{55}$$

$$s.t. \ \left|(\boldsymbol{W}_{RF})_{i,j}\right| = 1 \tag{56}$$

$$\|\boldsymbol{W}_{RF}\boldsymbol{W}_{BB}\|_F^2 \le P_T \tag{57}$$

Note that the columns of the unconstrained optimal digital beamforming matrix are mutually orthogonal in order to mitigate the interference between the multiplexed streams [38]. Inspired by this conclusion, we impose a similar constraint that the columns of the digital beamforming matrix $\boldsymbol{W}_{BB}$ should be mutually orthogonal, i.e.,

$$\boldsymbol{W}_{BB} = \rho \boldsymbol{W}_{DD} \tag{58}$$

$$\boldsymbol{W}_{BB}\boldsymbol{W}_{BB}^H = (\rho \boldsymbol{W}_{DD})(\rho \boldsymbol{W}_{DD})^H = \rho^2 \boldsymbol{I}_K \tag{59}$$

where $\boldsymbol{W}_{DD}$ is a unitary matrix with the same dimension as $\boldsymbol{W}_{BB}$.

By (58) and (59), the objective function in (55) can be further recast as:

$$\begin{aligned}
&\left\| \boldsymbol{B}_{opt}^* - \boldsymbol{W}_{RF}\boldsymbol{W}_{BB} \right\|_F^2 \\
&= \left(\mathrm{Tr}\left\{ \left(\boldsymbol{B}_{opt}^* - \boldsymbol{W}_{RF}\boldsymbol{W}_{BB} \right)^H \right\} \left(\boldsymbol{B}_{opt}^* - \boldsymbol{W}_{RF}\boldsymbol{W}_{BB} \right) \right)^2 \\
&= \mathrm{Tr}\left(\left(\boldsymbol{B}_{opt}^* \right)^H - \boldsymbol{W}_{BB}^H \boldsymbol{W}_{RF}^H \right) \left(\boldsymbol{B}_{opt}^* - \boldsymbol{W}_{RF}\boldsymbol{W}_{BB} \right) \\
&= \mathrm{Tr}\left(\left(\boldsymbol{B}_{opt}^* \right)^H \boldsymbol{B}_{opt}^* - \left(\boldsymbol{B}_{opt}^* \right)^H \boldsymbol{W}_{RF}\boldsymbol{W}_{BB} \right. \\
&\quad \left. - \boldsymbol{W}_{BB}^H \boldsymbol{W}_{RF}^H \left(\boldsymbol{B}_{opt}^* \right)^H + \boldsymbol{W}_{BB}^H \boldsymbol{W}_{RF}^H \boldsymbol{W}_{RF}\boldsymbol{W}_{BB} \right) \\
&= \mathrm{Tr}\left(\left(\boldsymbol{B}_{opt}^* \right)^H \boldsymbol{B}_{opt}^* \right) - 2\mathrm{Tr}\left(\left(\boldsymbol{B}_{opt}^* \right)^H \boldsymbol{W}_{RF}\boldsymbol{W}_{BB} \right) \\
&\quad + \mathrm{Tr}\left(\boldsymbol{W}_{BB}^H \boldsymbol{W}_{RF}^H \boldsymbol{W}_{RF}\boldsymbol{W}_{BB} \right) \\
&= \left\| \boldsymbol{B}_{opt}^* \right\|_F^2 - 2\rho\Re\left(\boldsymbol{W}_{DD} \left(\boldsymbol{B}_{opt}^* \right)^H \boldsymbol{W}_{RF} \right) \\
&\quad + \rho^2 \left\| \boldsymbol{W}_{RF}\boldsymbol{W}_{DD} \right\|_F^2
\end{aligned} \tag{60}$$

when $\rho = \frac{\Re\mathrm{Tr}\left(\boldsymbol{W}_{DD}\boldsymbol{B}_{opt}^*\boldsymbol{W}_{RF}\right)}{\|\boldsymbol{W}_{RF}\boldsymbol{W}_{DD}\|_F^2}$, the objective function in (60) can obtain the minimum value, i.e.,

$$\begin{aligned}
&\min_{\boldsymbol{W}_{RF},\boldsymbol{W}_{BB}} \left\| \boldsymbol{B}_{opt}^* - \boldsymbol{W}_{RF}\boldsymbol{W}_{BB} \right\|_F^2 \\
&= \left\| \boldsymbol{B}_{opt}^* \right\|_F^2 - \frac{\left\{ \Re\mathrm{Tr}\left(\boldsymbol{W}_{DD}\boldsymbol{B}_{opt}^*\boldsymbol{W}_{RF} \right) \right\}^2}{\|\boldsymbol{W}_{RF}\boldsymbol{W}_{DD}\|_F^2}
\end{aligned} \tag{61}$$

It is worth noting that it is challenging to deal with the product-form problem in the objective function in (61). To handle this challenge, we choose to add the constant term $\left(\frac{1}{2\|\boldsymbol{W}_{RF}\|_F^2} - 1\right)\left\|\boldsymbol{B}_{opt}^*\right\|_F^2 + \frac{1}{2}$ to the lower bound of the objective function in (61). Then, multiply it by the positive

constant term $2\|\boldsymbol{W}_{RF}\|_F^2$. So we have

$$\begin{aligned}
&\left\|\boldsymbol{B}_{opt}^*\right\|_F^2 \times 2\|\boldsymbol{W}_{RF}\|_F^2 - \frac{\left\{\Re\mathrm{Tr}\left(\boldsymbol{W}_{DD}\boldsymbol{B}_{opt}^*\boldsymbol{W}_{RF}\right)\right\}^2}{\|\boldsymbol{W}_{RF}\boldsymbol{W}_{DD}\|_F^2} \\
&\quad \times 2\|\boldsymbol{W}_{RF}\|_F^2 + \left[\left(\frac{1}{2\|\boldsymbol{W}_{RF}\|_F^2} - 1\right)\left\|\boldsymbol{B}_{opt}^*\right\|_F^2 + \frac{1}{2}\right] \\
&\quad \times 2\|\boldsymbol{W}_{RF}\|_F^2 \\
&= \left\|\boldsymbol{B}_{opt}^*\right\|_F^2 - 2\Re\mathrm{Tr}\left(\boldsymbol{W}_{DD}\boldsymbol{B}_{opt}^*\boldsymbol{W}_{RF}\right) + \|\boldsymbol{W}_{RF}\|_F^2 \\
&= \mathrm{Tr}\left(\boldsymbol{W}_{RF}^H\boldsymbol{W}_{RF}\right) - 2\Re\mathrm{Tr}\left(\boldsymbol{W}_{DD}\boldsymbol{B}_{opt}^*\boldsymbol{W}_{RF}\right) \\
&\quad + \mathrm{Tr}\left(\boldsymbol{W}_{DD}\left(\boldsymbol{B}_{opt}^*\right)^H\boldsymbol{B}_{opt}^*\boldsymbol{W}_{DD}^H\right) \\
&= \left\|\boldsymbol{B}_{opt}^*\boldsymbol{W}_{DD}^H - \boldsymbol{W}_{RF}\right\|_F^2 \qquad (62)
\end{aligned}$$

In conclusion, the problem P_1 can be recast as:

$$P_2: \quad \min_{\boldsymbol{W}_{RF},\boldsymbol{W}_{DD}} \left\|\boldsymbol{B}_{opt}^*\boldsymbol{W}_{DD}^H - \boldsymbol{W}_{RF}\right\|_F^2 \qquad (63)$$

$$s.t.\ \boldsymbol{W}_{DD}^H\boldsymbol{W}_{DD} = \boldsymbol{I}_K \qquad (64)$$

$$\left|(\boldsymbol{W}_{RF})_{i,j}\right| = 1 \qquad (65)$$

To handle the problem P_2, we adopt the AltOpt algorithm. The basic idea is as follows:

- Initializing a feasible analog beamforming matrix $\boldsymbol{W}_{RF}$ with random phase.
- Based on the fixed $\boldsymbol{W}_{RF}$ and (63), the calculation of $\boldsymbol{W}_{DD}$ can be modeled as:

$$\begin{aligned}
&\min_{\boldsymbol{W}_{DD}} \left\|\boldsymbol{B}_{opt}^*\boldsymbol{W}_{DD}^H - \boldsymbol{W}_{RF}\right\|_F^2 \\
&\qquad \Rightarrow \max_{\boldsymbol{W}_{DD}} \Re\mathrm{Tr}\left(\boldsymbol{W}_{DD}\boldsymbol{B}_{opt}^*\boldsymbol{W}_{RF}\right) \\
&s.t.\ (64) \qquad (66)
\end{aligned}$$

According to the definition of the dual norm and the Hölder's inequality, $\Re\mathrm{Tr}\left(\boldsymbol{W}_{DD}\boldsymbol{B}_{opt}^*\boldsymbol{W}_{RF}\right)$ can be further recast as

$$\begin{aligned}
&\Re\mathrm{Tr}\left(\boldsymbol{W}_{DD}\boldsymbol{B}_{opt}^*\boldsymbol{W}_{RF}\right) \\
&\le \left|\mathrm{Tr}\left(\boldsymbol{W}_{DD}\boldsymbol{B}_{opt}^*\boldsymbol{W}_{RF}\right)\right| \le \left\|\boldsymbol{W}_{DD}^H\right\|_\infty \cdot \left\|\left(\boldsymbol{B}_{opt}^*\right)^H\boldsymbol{W}_{RF}\right\|_1 \\
&= \left\|\left(\boldsymbol{B}_{opt}^*\right)^H\boldsymbol{W}_{RF}\right\|_1 = \sum_{k=1}^{K}\chi_k \qquad (67)
\end{aligned}$$

where $\{\chi_k\}_{k=1}^K$ represents the first K non-zero singular values of $\left(\boldsymbol{B}_{opt}^*\right)^H\boldsymbol{W}_{RF}$. According to (66) and (67), we can get that $\boldsymbol{W}_{DD} = \boldsymbol{V}\boldsymbol{U}_1^H$, $\mathbf{U}_1$ and $\mathbf{V}$ are the left and right unitary matrices, which are obtained by singular value decomposition (SVD) of matrix $\left(\boldsymbol{B}_{opt}^*\right)^H\boldsymbol{W}_{RF}$, i.e., $\left(\boldsymbol{B}_{opt}^*\right)^H\boldsymbol{W}_{RF} = \mathbf{U}_1\sum\boldsymbol{V}^H$.

Based on $\boldsymbol{W}_{DD}$, according to (63) and (65), the phases of matrix $\boldsymbol{W}_{RF}$ can be extracted from the phases of matrix $\boldsymbol{B}_{opt}^*\boldsymbol{W}_{DD}^H$, i.e.,

$$\arg\left(\boldsymbol{W}_{RF}\right) = \arg\left(\boldsymbol{B}_{opt}^*\boldsymbol{W}_{DD}^H\right) \qquad (68)$$

- Step 2 and step 3 are calculated alternately, until the convergence level or the maximum number of iterations is reached.
- Finally, we obtain the optimal $\boldsymbol{W}_{RF}^*$ and $\boldsymbol{W}_{DD}^*$, $\boldsymbol{W}_{BB}^* = \rho\boldsymbol{W}_{DD}^*$.

Algorithm Joint Design Algorithm of Digital Beamforming Matrix and Analog Beamforming Matrix

Input: Matrices $\{\boldsymbol{W}_{opt}\}_{k=1}^K$, initialize a feasible analog beamforming matrix $\boldsymbol{W}_{RF}^{(\delta=0)}$, iteration index $\delta = 0$, threshold $\varepsilon_4 = 10^{-3}$.

1. Obtain the maximum eigenvectors and corresponding eigenvalues of each $\boldsymbol{W}_{k,opt}$ by EVD of $\{\boldsymbol{W}_{opt}\}_{k=1}^K$.
2. Calculate $\boldsymbol{B}_{opt}^*$ by (54).
3. **Repeat**
4. For fixed $\boldsymbol{W}_{RF}^{(\delta)}$, SVD of $\left(\boldsymbol{B}_{opt}^*\right)^H\boldsymbol{W}_{RF}^{(\delta)}$, i.e., $\left(\boldsymbol{B}_{opt}^*\right)^H\boldsymbol{W}_{RF}^{(\delta)} = \mathbf{U}_1^{(\delta)}\sum\boldsymbol{V}^{H,(\delta)}$.
5. For fixed $\mathbf{U}_1^{(\delta)}$ and $\mathbf{V}^{(\delta)}$, calculate $\boldsymbol{W}_{DD}^{(\delta)} = \mathbf{V}^{(\delta)}\mathbf{U}_1^{H,(\delta)}$.
6. For fixed $\boldsymbol{W}_{DD}^{(\delta)}$, calculate $\boldsymbol{W}_{RF}^{(\delta+1)}$ by (68).
7. **Until** $\left\|\boldsymbol{B}_{opt}^*\boldsymbol{W}_{DD}^{H,(\delta)} - \boldsymbol{W}_{RF}^{(\delta)}\right\|_F^2 \le \varepsilon_4$.

Output: $\boldsymbol{W}_{RF}^*$, $\boldsymbol{W}_{BB}^* = \rho\boldsymbol{W}_{DD}^*$.

VI. COMPLEXITY AND CONVERGENCE ANALYSIS

A. COMPLEXITY ANALYSIS

The major complexity of the proposed algorithm is composed of nested iterative optimization and matrix decomposition, and both involve iterative optimization. The number of iterations depends on the predetermined convergence threshold, which is usually small. The complexity of the inner iteration algorithm mainly comes from the CCCP algorithm and the penalty function algorithm. In inner iterative algorithm, problem Q_8 is solved iteratively until it converges to the locally optimal solution. Then, the result obtained by the inner iteration algorithm is substituted into the outer iterative algorithm, to calculate the value of energy efficiency. Next, we update the variable $y$and continue to next iteration until the outer iterative algorithm converges to obtain the solution. To sum up, the complexity of proposed nested iterative optimization algorithm is approximately $O(I_oI_iI_pKM^3 + KM)$, where I_o, I_i and I_P are the numbers of iterations required in outer iterative algorithm, inner iterative algorithm and penalty function algorithm, respectively. The values of I_o, I_i and I_p are related to the predetermined convergence thresholds. In the joint design algorithm of digital beamforming matrix and analog beamforming matrix, the complexity mainly comes from alternating optimization in matrix decomposition. In the hybrid beamforming system, the dimension of the analog

beamforming matrix is much higher than that of the digital beamforming matrix. Therefor, the complexity of the algorithm is predominated by the analog beamforming part. In each iteration of the AltOpt algorithm, the update of the analog beamforming matrix is realized by a phase extraction operation of the matrix $\boldsymbol{B}_{opt}^{*}\boldsymbol{W}_{DD}^{H}$, whose dimension is $M \times K$. Therefor, the complexity of the matrix decomposition is approximately $O(I_m MK)$, where I_m is the number of iteration required in joint design algorithm of digital beamforming matrix and analog beamforming matrix. The value of I_m is related to the predetermined convergence threshold. To sum up, the complexity of the proposed algorithm is approximately $O(I_o I_i I_p KM^3 + KM + I_m MK)$, we can see that the level of complexity is not high.

B. CONVERGENCE ANALYSIS

In this section, we analyze the convergence of the proposed algorithm. In this paper, we mainly analyze the convergence of the inner and outer nested iterative algorithm, which affects the convergence of the proposed algorithm. In the inner iterative algorithm, problem Q_8 is a typical convex optimization problem, which can be iteratively solved. And the CCCP algorithm is a monotonically decreasing global optimization method, due to the characteristics of the CCCP algorithm, the inner iterative algorithm can be proved to be convergent [41]. For outer iterative algorithm, the optimization problem satisfies the convergence conditions mentioned in Section V-B of literature [32]. In addition, for the AltOpt algorithm, the optimization problem we proposed satisfies the convergence conditions mentioned in [37]. To sum up, the convergence of the proposed algorithm can be guaranteed.

TABLE 2. Simulation Parameters.

Parameters	Values	Parameters	Values
M	12*12	LP_{at}	0.017dB
K	16	N_{RF}	16
Rice factor	10	P_{RFC}	200mW
Bandwidth	50MHz	P_{PS}	30mW
Orbit altitude	1000km	P_{LO}	5mW
f	20GHz	P_{BB}	52mW
Power λ_k	144	P_{syn}	50mW

VII. SIMULATION RESULTS

In this section, we illustrate the performance of our proposed robust algorithm in the Massive MIMO LEO satellite communication system through numerical simulations. It is assumed that the variances of the channel errors are identical for different users, which are expressed as $\sigma_{\theta_k}^2 = \sigma_\theta^2$, $\sigma_{f_k}^2 = \sigma_f^2$. Without loss of generality, the SINR constraints are set to randomly generated between $0 \sim 5$dB for all users, e.q, $r_k \in (0 \sim 5\text{dB})$. In addition, the values of the adopted the other system parameters are listed in Table 2 [27]for clarity.

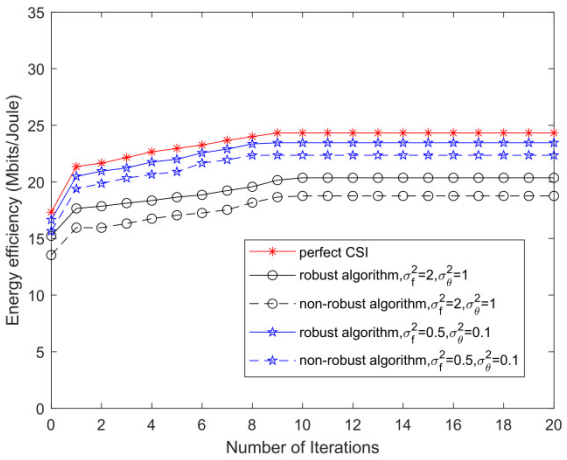

FIGURE 3. Convergence trajectory comparison of EE relative to different error parameters.

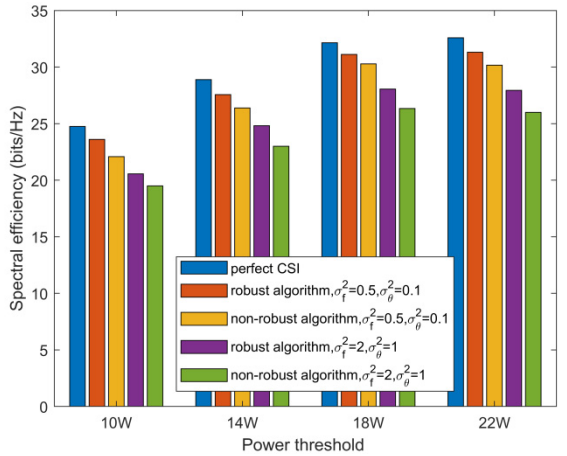

FIGURE 4. Comparison of the SE performance between the proposed robust algorithm and the conventional one. Results are presented versus the transmit power threshold for different system parameters.

Fig. 3 shows the convergence trajectory comparison of the proposed robust algorithm, versus the number of iterations for varying channel error variances. In this simulation, we set two different groups of channel error parameters, i.e., $\sigma_\theta^2 = 1$, $\sigma_f^2 = 2$, $\sigma_\theta^2 = 0.1, \sigma_f^2 = 0.5$. Let total transmit power be $P_T = 30W$. Meanwhile, we compare the proposed robust algorithm with the traditional non-robust algorithm. In addition, we take the EE under the perfect CSI as a comparison and reference. We can observe from the numerical results that the proposed algorithm can converge to stationary values within very few numbers of iterations, and its performance is better than the traditional non-robust algorithm. And the performance gains become more significant with larger variance of the channel errors.

Fig. 4 shows the SE performance of the proposed robust algorithm, the channel error parameters are set as above. We can observe from the numerical results that when the channel errors are small, the SE of the proposed algorithm

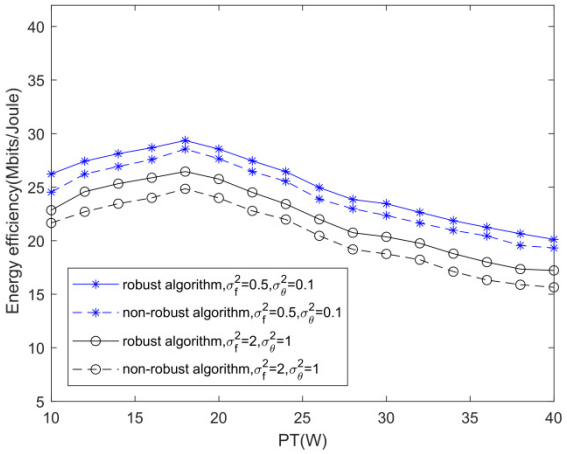

FIGURE 5. Comparison of the EE performance between the proposed robust algorithm and the conventional one. Results are presented versus the transmit power threshold for different system parameters.

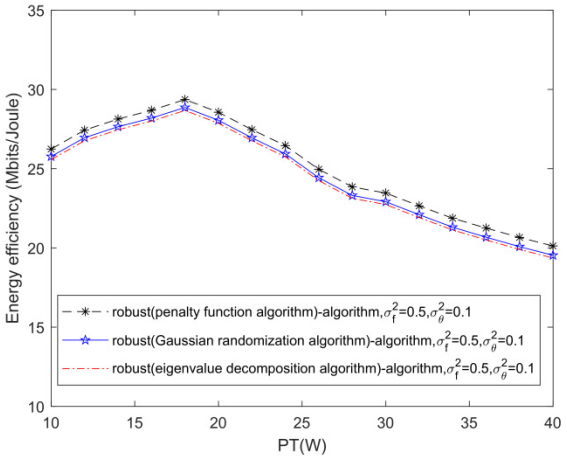

FIGURE 6. Comparison of the EE performance achieved by different algorithms (penalty function algorithm, Gaussian randomization algorithm, eigenvalue decomposition algorithm).

is close to that under the perfect CSI. And performance of the proposed algorithm is better than the traditional non-robust algorithm.

Fig. 5 shows the change trajectory of EE versus the transmit power threshold P_T, the channel error parameters are set as above. We can observe from the numerical results that the proposed robust algorithm is better than the conventional non-robust algorithm under different transmit power threshold. We can see that the EE values initially increase and then decreased as P_T increases. This is because the increment of power consumption is faster than that of the system rate.

Fig. 6 shows the EE performance comparison of the proposed penalty function algorithm with Gaussian randomization algorithm and eigenvalue decomposition algorithm [39]. We can observe from the numerical results that the proposed algorithm is better than the other two algorithms.

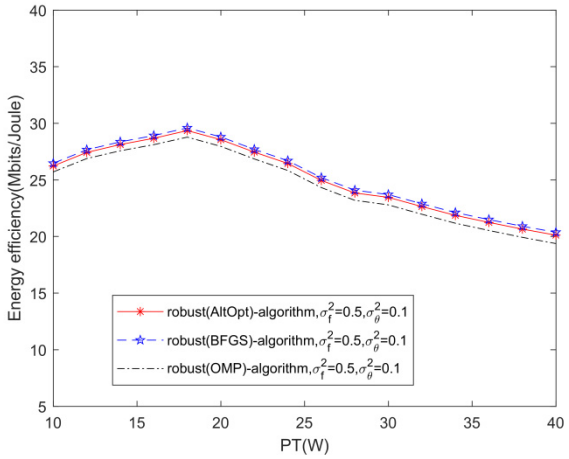

FIGURE 7. Comparison of the EE performance achieved by different algorithms (AltOpt algorithm, BFGS algorithm, OMP algorithm).

This is because the penalty function algorithm can get a better solution through iterative calculation, which can satisfy the rank-one constraint. Whereas the Gaussian randomization algorithm or eigenvalue decomposition algorithm calculates based on the variables that may not satisfy the rank-one constraint, which may obtain a solution with poor performance.

Fig. 7 shows the EE performance comparison of the proposed AltOpt algorithm with Broyden Fletcher Goldfarb Shanno (BFGS) [38] algorithm and orthogonal matching pursuit (OMP) [40] algorithm. We can observe from the numerical results that the performance of the proposed algorithm is close to the BFGS algorithm and better than the OMP algorithm. The performance of BFGS algorithm is close to the best, which is used as a reference here, but its algorithm complexity is high, and the complexity of each iteration is $O\left(MK^2 + 2K^3 + MK^2 + (M-1)K^2\right)$. In comparison, although the performance of the proposed AltOpt algorithm is slightly lower than that of BFGS algorithm, its algorithm complexity of each iteration is lower, i.e., $O(MK)$. Thus, the proposed algorithm has high cost-performance ratio.

VIII. CONCLUSION

In this paper, we have investigated a robust energy-efficient hybrid beamforming design for the Massive MIMO LEO satellite communication system. Taking the CSI errors caused by residual propagation delay and residual Doppler shift into account, we focused on the robust hybrid beamforming design to maximize the system EE under the constraints of transmit power and QoS. Firstly, we adopted the approximate ergodic user rate and the approximate ergodic SINR. Then, we invoked the SDP algorithm to transform the objective function equivalently. Meanwhile, we proposed an inner and outer nested iterative algorithm combining QTFP and CCCP to handle the nonconvex QCQP problem, and adopted the

penalty function algorithm to handle the rank-one constraint problem. Finally, we adopted the low complexity NFDM algorithm and AltOpt algorithm to obtain the digital beamforming matrix and the analog beamforming matrix. Numerical results have indicated that the performance of the robust algorithm performs better than that of the conventional one.

REFERENCES

[1] C. Jin, X. He, and X. Ding, "Traffic analysis of LEO satellite Internet of Things," in *Proc. 15th Int. Wireless Commun. Mobile Comput. Conf. (IWCMC)*, Jun. 2019, pp. 67–71.

[2] J. Chu and X. Chen, "Robust design for integrated satellite–terrestrial Internet of Things," *IEEE Internet Things J.*, vol. 8, no. 11, pp. 9072–9083, Jun. 2021.

[3] N. Gupta and S. Bitragunta, "Green satellite communication link design, optimization, and performance analysis," in *Proc. IEEE 7th Uttar Pradesh Sect. Int. Conf. Electr., Electron. Comput. Eng. (UPCON)*, Nov. 2020, pp. 1–5.

[4] J. Chu, X. Chen, C. Zhong, and Z. Zhang, "Robust design for NOMA-based multibeam LEO satellite Internet of Things," *IEEE Internet Things J.*, vol. 8, no. 3, pp. 1959–1970, Feb. 2021.

[5] L. You, J. Xiong, A. Zappone, W. Wang, and X. Gao, "Spectral efficiency and energy efficiency tradeoff in massive MIMO downlink transmission with statistical CSIT," *IEEE Trans. Signal Process.*, vol. 68, pp. 2645–2659, 2020.

[6] W. Wang, L. Gao, R. Ding, J. Lei, L. You, C. A. Chan, and X. Gao, "Resource efficiency optimization for robust beamforming in multi-beam satellite communications," *IEEE Trans. Veh. Technol.*, vol. 70, no. 7, pp. 6958–6968, Jul. 2021.

[7] X. Qiang, L. You, K.-X. Li, C. G. Tsinos, W. Wang, X. Gao, and B. Ottersten, "Hybrid A/D precoding for downlink massive MIMO in LEO satellite communications," in *Proc. IEEE Int. Conf. Commun. Workshops (ICC Workshops)*, Jun. 2021, pp. 1–6.

[8] C. Qi, H. Chen, Y. Deng, and A. Nallanathan, "Energy efficient multicast precoding for multiuser multibeam satellite communications," *IEEE Wireless Commun. Lett.*, vol. 9, no. 4, pp. 567–570, Apr. 2020.

[9] L. Gao, J. Ma, L. You, C. Pan, W. Wang, and X. Gao, "Robust energy-efficient multigroup multicast beamforming for multi-beam satellite communications," in *Proc. IEEE ICC*, Dublin, Ireland, Jun. 2020, pp. 1–6.

[10] X. Guo, D. Yang, Z. Luo, H. Wang, and J. Kuang, "Robust THP design for energy efficiency of multibeam satellite systems with imperfect CSI," *IEEE Commun. Lett.*, vol. 24, no. 2, pp. 428–432, Feb. 2020.

[11] R. T. Schwarz, T. Delamotte, K.-U. Storek, and A. Knopp, "MIMO applications for multibeam satellites," *IEEE Trans. Broadcast.*, vol. 65, no. 4, pp. 664–681, Dec. 2019.

[12] L. Lu, G. Y. Li, A. L. Swindlehurst, A. Ashikhmin, and R. Zhang, "An overview of massive MIMO: Benefits and challenges," *IEEE J. Sel. Topics Signal Process.*, vol. 8, no. 5, pp. 742–758, Oct. 2014.

[13] L. You, K.-X. Li, J. Wang, X. Q. Gao, X.-G. Xia, and B. Ottersten, "LEO satellite communications with massive MIMO," in *Proc. IEEE ICC*, Dublin, Ireland, Jun. 2020, pp. 1–6.

[14] S. Jain, A. Markan, and C. Markan, "Performance evaluation of a millimeter wave MIMO hybrid beamforming system," in *Proc. IEEE Latin-Amer. Conf. Commun. (LATINCOM)*, Nov. 2020, pp. 1–5.

[15] L. Cheng, G. Yue, Z. Wang, and S. Li, "Low-complexity wideband channel estimation for millimeter-wave massive MIMO systems via joint parameter learning," in *Proc. IEEE 92nd Veh. Technol. Conf. (VTC-Fall)*, Nov. 2020, pp. 1–5.

[16] Y. Zhang, Y. Wu, A. Liu, X. Xia, T. Pan, and X. Liu, "Deep learning-based channel prediction for LEO satellite massive MIMO communication system," *IEEE Wireless Commun. Lett.*, vol. 10, no. 8, pp. 1835–1839, Aug. 2021.

[17] L. You, K.-X. Li, J. Wang, X. Gao, X.-G. Xia, and B. Ottersten, "Massive MIMO transmission for LEO satellite communications," *IEEE J. Sel. Areas Commun.*, vol. 38, no. 8, pp. 1851–1865, Aug. 2020.

[18] I. Ali, N. Al-Dhahir, and J. E. Hershey, "Doppler characterization for LEO satellites," *IEEE Trans. Commun.*, vol. 46, no. 3, pp. 309–313, Mar. 1998.

[19] M. Xu, Y. He, C. Wang, G. Cui, and W. Wang, "Doppler rate estimation scheme for UFMC based LEO satellite communication system," in *Proc. IEEE Int. Conf. Commun. Syst. (ICCS)*, Dec. 2016, pp. 1–5.

[20] Q. Wei, X. Chen, and Y. F. Zhan, "Exploring implicit pilots for precise estimation of LEO satellite downlink Doppler frequency," *IEEE Commun. Lett.*, vol. 24, no. 10, pp. 2270–2274, Oct. 2020.

[21] S. Kay and S. Saha, "Mean likelihood frequency estimation," *IEEE Trans. Signal Process.*, vol. 48, no. 7, pp. 1937–1946, Jul. 2000.

[22] A. Gharanjik, M. R. B. Shankar, P.-D. Arapoglou, M. Bengtsson, and B. Ottersten, "Precoding design and user selection for multibeam satellite channels," in *Proc. IEEE SPAWC*, Stockholm, Sweden, Jun. 2015, pp. 420–424.

[23] G. Taricco, "Linear precoding methods for multi-beam broadband satellite systems," in *Proc. 20th Eur. Wireless Conf.*, Barcelona, Spain, May 2014, pp. 1–6.

[24] M. A. Albreem, A. H. A. Habbash, A. M. Abu-Hudrouss, and S. S. Ikki, "Overview of precoding techniques for massive MIMO," *IEEE Access*, vol. 9, pp. 60764–60801, 2021.

[25] V. M. Vergara and S. E. Barbin, "LOS and NLOS capacity components in MIMO Rice fading channels," in *Proc. Asia–Pacific Microw. Conf.*, 2010, pp. 1589–1592.

[26] L. Gao, W. Wang, R. Ding, L. You, and X. Gao, "Resource efficiency optimization for robust multigroup multicast satellite communications," in *Proc. IEEE ICC*, Montreal, QC, Canada, Jun. 2021, pp. 1–6.

[27] M. Mahmood, A. Koc, and T. Le-Ngoc, "Energy-efficient MU-massive-MIMO hybrid precoder design: Low-resolution phase shifters and digital-to-analog converters for 2D antenna array structures," *IEEE Open J. Commun. Soc.*, vol. 2, pp. 1842–1861, 2021, doi: 10.1109/OJCOMS.2021.3101747.

[28] L. Dong, W. Wenbo, and L. Yonghua, "Monte Carlo simulation with error classification for multipath Rayleigh fading channel," in *Proc. Int. Conf. Telecommun.*, 2009, pp. 223–227.

[29] M. Bengtsson and B. Ottersten, "Optimal and suboptimal transmit beamforming," in *Handbook of Antennas in Wireless Communications*. Boca Raton, FL, USA: CRC Press, 2001.

[30] Q. Li, Y. Liu, M. Shao, and W.-K. Ma, "Proximal distance algorithm for nonconvex QCQP with beamforming applications," in *Proc. IEEE Int. Conf. Acoust., Speech Signal Process. (ICASSP)*, May 2020, pp. 5155–5159.

[31] E. Song, H. Zhou, Y. Zhu, and Q. Shi, "Some results on semidefinite programming with rank constraint," in *Proc. IEEE Int. Conf. Prog. Informat. Comput.*, Dec. 2010, pp. 1134–1137.

[32] K. Shen and W. Yu, "Fractional programming for communication systems—Part I: Power control and beamforming," *IEEE Trans. Signal Process.*, vol. 66, no. 10, pp. 2616–2630, May 2018.

[33] Y. Sun, P. Babu, and D. P. Palomar, "Majorization-minimization algorithms in signal processing, communications, and machine learning," *IEEE Trans. Signal Process.*, vol. 65, no. 3, pp. 794–816, Feb. 2017.

[34] A. Kachouh, Y. Nasser, and H. A. Artail, "On the capacity optimization of D2D underlying cellular communications," in *Proc. 23rd Int. Conf. Telecommun. (ICT)*, May 2016, pp. 1–5.

[35] Z.-Q. Luo, W.-K. Ma, A. M.-C. So, Y. Ye, and S. Zhang, "Semidefinite relaxation of quadratic optimization problems," *IEEE Signal Process. Mag.*, vol. 27, no. 3, pp. 20–34, May 2010.

[36] J. G. McWhirter, P. D. Baxter, T. Cooper, S. Redif, and J. Foster, "An EVD algorithm for para-Hermitian polynomial matrices," *IEEE Trans. Signal Process.*, vol. 55, no. 5, pp. 2158–2169, May 2007, doi: 10.1109/TSP.2007.893222.

[37] X. Yu, J.-C. Shen, J. Zhang, and K. B. Letaief, "Alternating minimization algorithms for hybrid precoding in millimeter wave MIMO systems," *IEEE J. Sel. Topics Signal Process.*, vol. 10, no. 3, pp. 485–500, Apr. 2016.

[38] J. Jin, Y. R. Zheng, W. Chen, and C. Xiao, "Hybrid precoding for millimeter wave MIMO systems: A matrix factorization approach," *IEEE Trans. Wireless Commun.*, vol. 17, no. 5, pp. 3327–3339, May 2018.

[39] L. Gao, J. Ma, L. You, C. Pan, W. Wang, and X. Gao, "Robust energy-efficient multigroup multicast beamforming for multi-beam satellite communications," in *Proc. IEEE Int. Conf. Commun. (ICC)*, Jun. 2020, pp. 1–6.

[40] O. El Ayach, S. Rajagopal, S. Abu-Surra, Z. Pi, and R. W. Heath, Jr., "Spatially sparse precoding in millimeter wave MIMO systems," *IEEE Trans. Wireless Commun.*, vol. 13, no. 3, pp. 1499–1513, Mar. 2014.

[41] T. Lipp and S. Boyd, "Variations and extension of the convex-concave procedure," *J. Optim. Eng.*, vol. 17, no. 2, pp. 263–287, 2016.

[42] J. Palacios, N. Gonzalez-Prelcic, C. Mosquera, T. Shimizu, and C.-H. Wang, "A hybrid beamforming design for massive MIMO LEO satellite communications," 2021, *arXiv:2104.11158*.
[43] M. Lin, Z. Lin, W.-P. Zhu, and J.-B. Wang, "Joint beamforming for secure communication in cognitive satellite terrestrial networks," *IEEE J. Sel. Areas Commun.*, vol. 36, no. 5, pp. 1017–1029, May 2018.
[44] J. Ouyang, M. Lin, Y. Zou, W.-P. Zhu, and D. Massicotte, "Secrecy energy efficiency maximization in cognitive radio networks," *IEEE Access*, vol. 5, pp. 2641–2650, 2017.
[45] A. H. Phan, H. D. Tuan, H. H. Kha, and D. T. Ngo, "Nonsmooth optimization for efficient beamforming in cognitive radio multicast transmission," *IEEE Trans. Signal Process.*, vol. 60, no. 6, pp. 2941–2951, Jun. 2012.

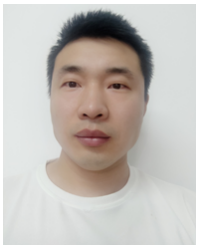

YANG LIU is currently pursuing the master's degree with Space Engineering University, China. His research interests include satellite communications, mobile communications, multi-antenna technology, and fixed communications. He has rich practical experience in communications.

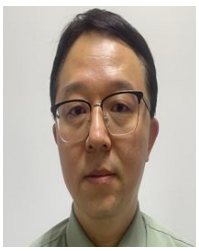

CHANGQING LI received the Ph.D. degree in communication engineering.

He is currently a Professor at Space Engineering University, China. His current research interests include satellite communications, mobile communications, 5G communication technology, and antenna technology.

JIONG LI received the Ph.D. degree in communication engineering.

He is currently a Lecturer at Space Engineering University, China. His current research interests include satellite communications, mobile communications, anti jamming communications, and antenna technology.

LU FENG is currently pursuing the master's degree with Space Engineering University, China. His research interests include satellite communications and anti-jamming communications. He has rich practical experience in communications.